Journal of Applied Polymer Science

Effect of glass transition temperature and saturation temperature on the solid-state microcellular foaming of cyclic olefin copolymer

Huimin Guo, Vipin Kumar
Department of Mechanical Engineering, University of Washington, Washington 98195
Correspondence to: H. Guo (E-mail: hmguo@uw.edu)

ABSTRACT: Effect of glass transition temperature and saturation temperature on the solid-state microcellular foaming of cyclic olefin copolymer (COC)—including CO_2 solubility, diffusivity, cell nucleation, and foam morphology—were investigated in this article. COCs of low T_g (78°C) and high T_g (158°C) were studied. Solubilities are 20–50% higher in high T_g COC than in the low T_g COC across the saturation temperature range. Diffusivities are about 15% higher on average in high T_g COC for temperatures up to 50°C. A much faster increase of diffusivity beyond 50°C is observed in low T_g COC due to it being in the rubbery state. Under similar gas concentration, high T_g COC starts foaming at a higher temperature. And the foam density decreases faster in low T_g COC with foaming temperature. Also, high T_g COC foams show about two orders of magnitude higher cell nucleation density than the low T_g COC foams. The effect of saturation temperature on microcellular foaming can be viewed as the effect of CO_2 concentration. Nucleation density increases and cell size decreases exponentially with increasing CO_2 concentration. Uniform ultramicrocellular structure with an average cell size of 380 nm was created in high-T_g COC. A novel hierarchical structure composed of microcells (2.5 μm) and nanocells (cell size 80 nm) on the cell wall was discovered in the very low-density high-T_g COC foams. © 2015 Wiley Periodicals, Inc. J. Appl. Polym. Sci. **2015**, *132*, 42226.

KEYWORDS: foams; glass transition; nanostructured polymers; porous materials; thermoplastics

Received 10 October 2014; accepted 13 March 2015
DOI: 10.1002/app.42226

INTRODUCTION

Microcellular foams are thermoplastic foams with cells on the order of 10 μm, which was conceived at MIT three decades ago.[1,2] In a pioneering paper, Martini *et al.*[2] described a two-step process to create microcellular structure in high-impact polystyrene, that involved saturating the polymer with a nonreacting gas and then heating the gas laden polymer to near the glass transition temperature. This process is later known as the solid-state process, as the polymer foam is created near the T_g of the gas–polymer system, well below the melting point. This process has been used to investigate a number of polymers, including PVC,[3] ABS,[4] PC,[5] PET,[6] and PLA,[7,8] to name a few. In a variation of this process, microcellular foams have been created by a sudden drop in gas pressure that causes a solubility drop resulting in a cell nucleation.[9]

The effect of T_g on the microcellular foaming of polymers has not been studied previously. The fact that T_g of cyclic olefin copolymer (COC) can be easily customized over a wide range by altering its norbornene content provides us an opportunity to study the effect of T_g on microcellular foaming process.

COC is a family of amorphous copolymers of ethylene and norbornene. COC with higher norbornene content has higher T_g due to the increased chain rigidity. In contrast to polyethylene, which shows poor solid-state foaming behavior due to low gas solubility and high crystallinities, COC generally presents good foaming behaviors, due to the fact that the introduction of bulky norbornene groups into the main chains prevents the crystallization of ethylene. COC has low water absorption, excellent water vapor barrier properties, high chemical resistance, and low shrinkage. It also shows excellent optical properties, such as low birefringence and high transparency, and is a competitor to conventional engineering plastics, such as polycarbonate.[10] The current usage of COC resins include transparent moldings for optical data storage, lenses, sensors, and industrial products in the construction and lighting sectors. There is also interest in packaging for pharmaceuticals, medical devices, and diagnostic disposable.

A few groups have explored microcellular foaming of COC. Processing using CO_2 as a blowing agent has been successfully done in thin films of 6013 COC (T_g of 139°C) by Krause *et al.*[11] They saturated films at room temperature with CO_2 at 5 MPa which resulted in a 4.3 wt % CO_2. Foaming was carried out between 65 and 155°C, and foams with a cell size <5 μm and cell densities on the order of 10^{11} cells/cm^3 were achieved.

Table I. Materials Used in This Study

Commercial name	T_g (°C)	Density (g/cc)	Norbornene content (mol %)[20]	Designated in this paper as
TOPAS 8007	78	1.02	40	COC78
TOPAS 6015	158	1.02	54	COC158

Sun *et al.*[12] saturated COC (T_g of 137°C) in pressure up to 30 MPa at 100–180°C, and foamed utilizing the pressure-quench method. They achieved foams with cell densities on the order of 10^{10} cells/cm^3 range and cell size about 2–5 μm for the samples that were rapidly cooled in ice-water bath. Gendron *et al.*[13] have explored solid-sate foaming of TOPAS COC 8007 and 5013 (T_g 78 and 135°C, respectively). The samples were saturated in a pressure ranging from 1.4 to 5.9 MPa to a CO_2 concentration of between 2 and 8 wt %. Foaming was then carried out by biaxially stretching and simultaneously heating the samples. Recently, Chen *et al.*[14] investigated solid-state foaming of TOPAS 6017 COC (T_g of 180°C) in the pressure range of 5–10 MPa at 40°C. The resulting COC foams had a cell size in the range of 0.3–7.5 μm and cell density ranging from 10^9 to 10^{12} cells/cm^3. Also, the transition from foaming to crazing under certain conditions due to stress field was identified.

Besides the effect of T_g, the effect of saturation temperature (T_{sat}) on the microcellular foaming and foam morphology is not well established, especially in the subcritical regime. In most of microcellular foaming studies, T_{sat} has been kept constant during the saturation step. Typically, room temperature has been used in the subcritical regime. A higher T_{sat} enables a faster diffusion (thus short sorption time), which is beneficial to the production process; on the other hand, a higher T_{sat} results in a lower solubility of gas in polymer.[15–17] Solubility is known to significantly influence cell nucleation and resulting microstructures.[18,19] Thus, to create foams with desired structures and properties, the effect of T_{sat} on the foaming and final foam morphology need to be established.

In this article, we compare the solid-state microcellular foaming of COCs with a high and low T_g, with the T_{sat} varying from 20 to 80°C. The effect of T_g and T_{sat} on CO_2 solubility, diffusivity, cell nucleation, and foam morphology are reported.

EXPERIMENTAL

Materials

Two grades of COC, grade 8007 and 6015, were provided by TOPAS Advanced Polymers Inc. COC sheets of 0.25 mm thickness were cut into 2.5 × 2.5 cm samples for sorption and foaming studies. T_g and density of both materials are listed in Table I. CO_2 with 99.9% purity was provided by Praxair, Inc.

Sorption

Sorption experiments were conducted by placing samples in a pressure vessel maintained at 5 MPa with an accuracy of ±0.1 MPa. Sorption temperatures (T_{sat}) varied over a range from 20 to 80°C. For sorption experiment above room temperature, a heating jacket wrapped around the pressure vessel and a temperature controller was used to maintain the pressure vessel at a desired temperature. During saturation, samples were periodically taken out from the pressure vessel, and weighed on a Mettler AE240 analytical scale accurate to ±10 μg. Samples were then promptly put back to the pressure vessel and repressurized. The sorption experiment continued until no further weight increase was observed in the specimen.

Foaming

Specimens used for foaming studies were first wrapped in porous paper towel, and then placed in a pressure vessel which was maintained at 5 MPa. Samples were kept in the pressure vessel for 10 h to ensure the full absorption of CO_2. After full saturation, samples were immediately removed from the pressure vessel, and quickly transferred to and immersed in a hot silicone oil bath (Thermo Haake B5) set at a desired temperature. The foaming time used for all samples was 30 s. After foaming, the sample was immediately quenched in room temperature water to stop further foaming.

Characterization

The excess silicone oil was removed from the surface of the sample before any characterization. The density of each sample was determined according to ASTM D792 using Mettler AE240 analytical scale. Samples were allowed to desorb for at least 1 week before density measurement was performed in order to eliminate the effect of residual CO_2. A representative set of samples were imaged with a scanning electron microscope (SEM) to examine the microstructures produced. All images were taken on an FEI Sirion SEM. Samples were first scored with a razor blade and freeze fractured with liquid nitrogen to expose the cross-section. They were then coated with Au/Pd for 90 s at a current of 18 mA. Micrographs were taken at the center of the cross section of the specimen and analyzed using software ImageJ (National Institute of Health, USA). Average cell size was calculated by taking average cell diameters of at least 50 cells in the SEM micrographs. Cell nucleation density (number of cells nucleated per cubic centimeter of the unfoamed sample) was calculated using a procedure described in literature.[18]

RESULTS AND DISCUSSION

Effect of T_g and T_{sat} on CO_2 Solubility

CO_2 solubility is defined as the equilibrium CO_2 concentration for each specific saturation condition. CO_2 concentration is usually expressed as a percentage of the original polymer mass, e.g., 10% CO_2 concentration means that 10% of the mass of original polymer is now absorbed into the polymer. There was a short time interval between the pressure release and weight measurement in the sorption experiment. To account for the CO_2 loss during this interval, the solubility of CO_2 in the samples was obtained by extrapolating the desorption curve to zero desorption time. Detailed procedures can be found in literature.[21,22] Solubility for both COC78 and COC158 at different saturation temperatures are summarized in Table II and plotted in Figure 1.

We can see that as T_{sat} increases, the solubility for both COCs decreases. Also, we can see that the higher T_g COC has a higher solubility in every saturation temperature. Hu *et al.*[20] measured

Table II. Summary of Solubility and Diffusivity for COC78 and COC158

	Solubility (%)		Diffusivity (cm^2/s)	
T_{sat} (°C)	COC78	COC158	COC78	COC158
20	5.40	7.80	1.23×10^{-8}	1.43×10^{-8}
40	4.16	5.62	2.40×10^{-8}	2.84×10^{-8}
50	3.84	5.05	3.46×10^{-8}	3.80×10^{-8}
60	3.45	4.40	7.55×10^{-8}	4.91×10^{-8}
70	3.25	4.04	1.63×10^{-7}	6.83×10^{-8}
80	3.07	3.76	2.78×10^{-7}	9.08×10^{-8}

the solubility of four different COCs with T_g varying between 81 and 173°C and conducted sorption experiments up to 3.2 MPa at room temperature. They reported higher solubilities in higher T_g COC. The higher solubility was believed to be due to the larger free volume in the higher T_g COC. Bulky norbornene on the backbone disrupt the chain packing, thereby increasing the free volume. The measured fractional free volume at room temperature was 0.119 for 154°C T_g COC and 0.062 for 81°C T_g.[20]

Also, solubilities of both COCs seem to converge at high saturation temperatures. This might be due to the decreasing free volume in both COCs as the temperature increases. A higher temperature allows higher chain mobility and thus less unoccupied free volume.

The temperature dependence of solubility is typically given by Arrhenius equation,[15,16,23]

$$S = S_0 \exp\left(-\frac{\Delta H_S}{RT}\right) \quad (1)$$

where S_0 is the pre-exponential factor, ΔH_S is the heat of sorption or enthalpy change upon solution of gas in the polymer, and R is the gas constant.

Figure 2 shows the natural logarithm of solubilities as a function of the reciprocal of saturation temperature. A linear trend

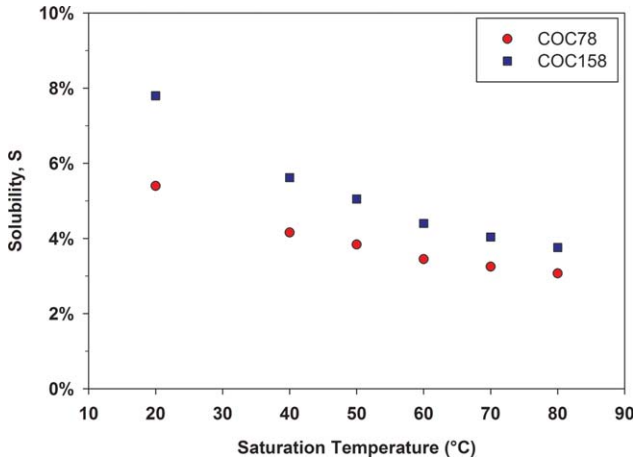

Figure 1. Solubility of COC78 and COC158 at different saturation temperatures. [Color figure can be viewed in the online issue, which is available at wileyonlinelibrary.com.]

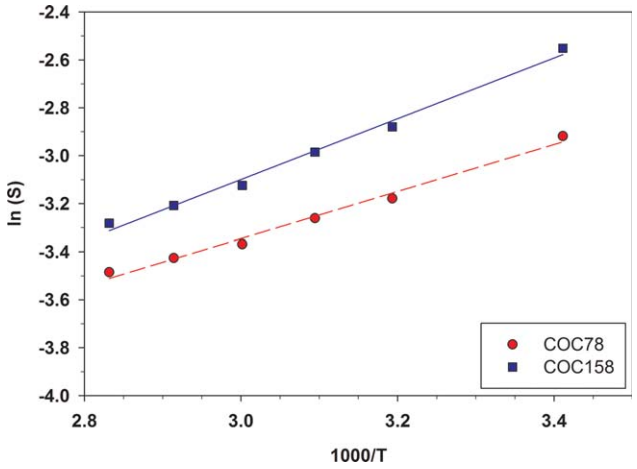

Figure 2. Natural logarithm of solubility as a function of reciprocal of saturation temperature for COC78 and COC158. Two best-fit lines are also included. [Color figure can be viewed in the online issue, which is available at wileyonlinelibrary.com.]

can be seen for both grades of COC. From the slopes, we calculated the heat of sorption to be −8.2 and −10.5 kJ/mol for COC78 and COC158, respectively. Negative values indicate the exothermic nature of the sorption of CO_2 in COC. By comparing the two heats of sorption, we observe a larger heat release from the sorption of CO_2 in higher T_g COC.

Effect of T_g and T_{sat} on CO_2 Diffusivity

One of the commonly used methods to determine diffusivity from a sorption plot is the initial slope method, which uses the slope of the initial part of a normalized sorption plot. At sufficiently short sorption times, the total mass uptake of gas in thin sheets can be described by[24]

$$\frac{M_t}{M_i} = \frac{4}{L}\left(\frac{Dt}{\pi}\right)^{0.5} \quad (2)$$

where M_t is the amount of gas absorbed into polymer at time t, M_i is the equilibrium concentration, D is the diffusivity (cm^2/s), and L is the polymer thickness (cm). Diffusivity can then be calculated from the slope R of the early part of M_t/M_i vs $t^{0.5}/L$ plots.

$$D = \frac{\pi R^2}{16} \quad (3)$$

In Figure 3, we have plotted the early part of the CO_2 uptake curves in COC78 with the time axis normalized for thickness, in units of ($t^{0.5}/L$), where t is in seconds and L is in centimeters. From the slopes, we can obtain sorption diffusivities using eq. (3). Similarly, we can get sorption diffusivities for COC158. Both are summarized in Table II.

From the data, we see that as T_{sat} increases, diffusivity also increases. The effect of temperature on the diffusivity of gas in polymers was first shown by Barrer[25] and later confirmed by others[15,16] to be that of an activated process obeying the Arrhenius relationship:

$$D = D_0 \exp\left(-\frac{\Delta H_D}{RT}\right) \quad (4)$$

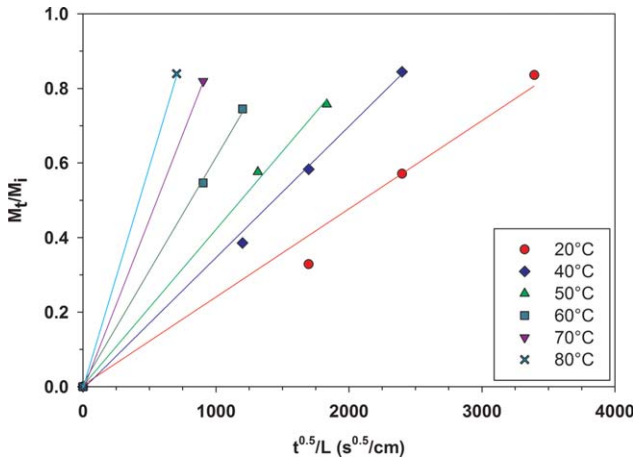

Figure 3. Early parts of sorption curves for COC78 at different saturation temperatures. [Color figure can be viewed in the online issue, which is available at wileyonlinelibrary.com.]

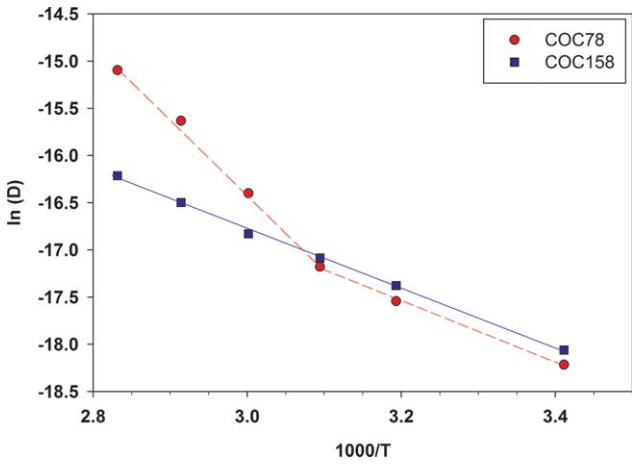

Figure 4. Natural logarithm of diffusivities as a function of reciprocal of saturation temperature for COC78 and COC158. [Color figure can be viewed in the online issue, which is available at wileyonlinelibrary.com.]

where D_0 is the pre-exponential factor, ΔH_D is the activation energy for diffusion, R is the gas constant, and T is the temperature in Kelvin.

Figure 4 shows the natural logarithm of sorption diffusivities as a function of the reciprocal of saturation temperature. A single linear trend can be observed for COC158, with an activation energy of 26.2 kJ/mol. However, for COC78, there exist two different linear lines for temperatures above and below 50°C, with a larger slope for above 50°C case. The activation energy of diffusion is calculated to be 66.7 and 27 kJ/mol, for the temperature above and below 50°C, respectively.

When below 50°C, COC78 has similar diffusivities and activation energy as the COC158. Segmental chain mobility and free volume likely influence the diffusion process of CO_2 in polymer. A higher segmental chain mobility enables a faster diffusion, and larger free volume also enables a faster diffusion. Compared to COC78, COC158 has lower segmental chain mobility, but higher free volume. These two influence the diffusion in opposite ways. The net effect is a slightly higher diffusivity and lower activation energy in COC158.

The sudden change of activation energy at 50°C for COC78 is probably due to the glass transition happening around this temperature. Absorption of CO_2 depresses the T_g of polymer. At around 50°C, the amount of CO_2 absorbed sufficiently depresses T_g of COC78 to below the saturation temperature, and as a result, the polymer is in the rubbery state.

The phenomenon that higher activation energy is needed when polymer is in rubbery state was previously reported and explained by Meares[26] in the diffusion of O_2 and Ar in polyvinyl acetate. The higher activation energy in the rubbery state is due to a larger zone of activation. Above T_g, gas molecules which dissolve in the polymer must create their own "holes" by separating the interchain polymer contacts. The penetrant then diffuses through the polymer matrix along cylindrical voids created by the synchronized rotation of polymer segments about the C—C bonds. Below T_g, the polymer consists of regions of densely packed and arranged chains which have limited freedom for rotation, separated by less dense regions of disordered chains that form the "holes" into which the gas absorbs. The gas molecule diffusion between the holes by slight compressing of localized chains in the dense regions enabling the gas molecules to pass through. The compression in the glassy state does not create the long cavities common to the rubbery state, indicating that the zone of chains activation is much larger in the rubbery state.

Effect of T_g on Foaming and Foam Morphology

From the solubility study above, we know that at the same saturation temperature, COC78 and COC158 have different CO_2 solubilities. Gas concentration is one of the most significant factors affecting the cell nucleation.[18,19] In order to decouple the T_g effect and gas concentration effect, we need to first saturate both grades of COC with a similar level of CO_2 concentration. COC78 was saturated at 20°C to achieve a CO_2 concentration of 5.4%, and COC158 at 40°C to get 5.62% CO_2 concentration.

Samples were then foamed in a range of foaming temperature. Figure 5 shows the relative density for both COC78 and COC158. The same general trend of decreasing density with the increasing foaming temperature up to a certain temperature is observed. Afterward, relative density increases with a further increase in the foaming temperature. This has been previously observed in other polymer–gas systems[3,4,27] and was attributed to the cell collapse at higher foaming temperatures.

The threshold foaming temperature, i.e., minimum temperature for foaming to occur, is 50°C for COC78 and 90°C for COC158. The similar gas concentration in these two COCs introduces a similar plasticization effect. However, the high T_g COC has more rigid chain and less chain mobility to start with, thus a higher threshold foaming temperature in higher T_g COC can be expected.

The density decrease is slightly steeper in the COC78. It takes about 50°C increase in foaming temperature to reduce the relative density from 100% down to 20%, whereas 80°C is needed for COC158 to reach the same density reduction. The nucleated

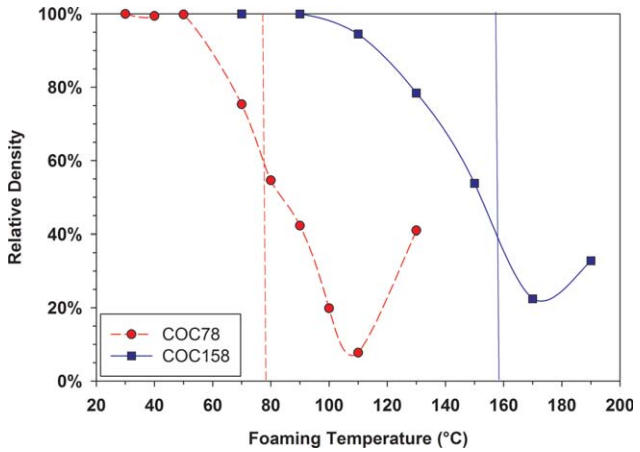

Figure 5. Relative density curves for COC78 and COC158, with two vertical lines indicating the two T_gs. [Color figure can be viewed in the online issue, which is available at wileyonlinelibrary.com.]

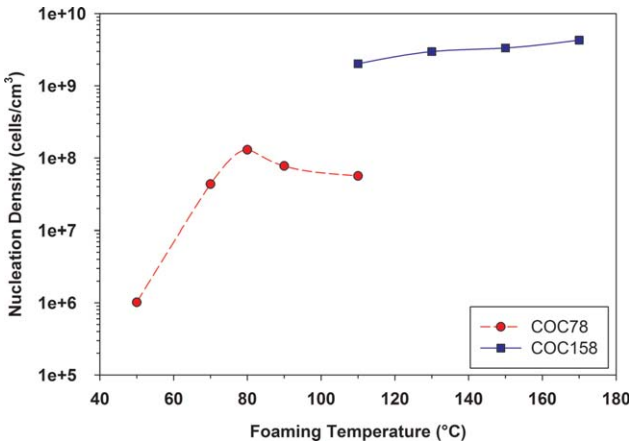

Figure 6. Nucleation density at different foaming temperatures for COC78 and COC158. [Color figure can be viewed in the online issue, which is available at wileyonlinelibrary.com.]

cells grow to a certain size upon heating at a given foaming temperature. The final cell size is a complex function of gas saturation temperature and pressure, the polymer T_g, polymer matrix viscosity and extensional viscosity and its dependence on temperature, and the foaming temperature. The observation that for the higher T_g COC, a larger temperature increase is needed to reduce the density from 100 to 20% can be explained by the fact that the viscosity of the COC158 is higher than that of the COC78. Thus, a higher temperature is needed to achieve the cell growth that corresponds to a 20% relative density.

Figures 6 and 7 compare the nucleation density and average cell size of COC78 and COC158 foams. An enhanced cell nucleation can be observed in the COC158. The cell nucleation density is on the order of 10^9 cells/cm^3 for COC158, whereas for COC78 the nucleation density is mostly on the order of 10^7 cells/cm^3. Almost two orders of magnitude higher nucleation density is achieved in the higher T_g COC. The mechanism for a higher nucleation density in the higher T_g COC is not yet understood and is a subject of continuing investigation. Smaller cell size is seen in higher T_g COC. Cell size of COC158 is between 3 and 10 μm, whereas COC78 has a cell size from 10 μm up to 60 μm. SEM images of representative samples of both grades are shown in Figure 8. At similar densities, COC158 has a much smaller cell size than COC78.

Effect of T_{sat} on Foaming and Foam Morphology

The high T_g COC158 was selected to study the effect of saturation temperature on microcellular foaming. From the sorption study, we know that saturation temperature affects the solubility (Table II). The effect of saturation temperature can be viewed as the effect of gas concentration. Samples were initially saturated at 60, 40, and 20°C, and CO_2 concentration of 4.4, 5.62, and 7.8% were achieved, respectively.

Figure 9 shows the relative density of foams saturated at different temperatures and then foamed in a range of temperatures. At higher saturation temperature, the CO_2 concentration is lower. A higher threshold foaming temperature is needed, and a more rapid decrease of relative density with foaming temperature is observed. Figures 10 and 11 show the nucleation density and average cell size as a function of CO_2 concentration. The straight trend line indicates that nucleation density increases exponentially with CO_2 concentration. Similar exponential relationship was reported in other polymer–gas systems.[15,16] Also, average cell size decreases exponentially with increasing CO_2 concentration. At 7.8% CO_2, cell size falls below 1 μm into the ultramicrocellular region. The smallest cell size is about 380 nm. Figure 12 shows the microstructures of representative samples that were saturated at different temperatures and then foamed at 130°C.

A novel hierarchical structure (Figure 13) is observed in the very low-density foams. This sample was first saturated at 20°C and then foamed at 170°C. It has a relative density of 9.1%. The hierarchical structure consists of microcells with cell size about 2.5 μm and nanopores with cell size about 80 nm. The cell wall is only about 50 nm in thickness. The spaces enclosed by the cell walls of the microcells are interconnected through the nanopores. This novel structure may possess some unique thermal insulation, sound absorption, and filtration properties.

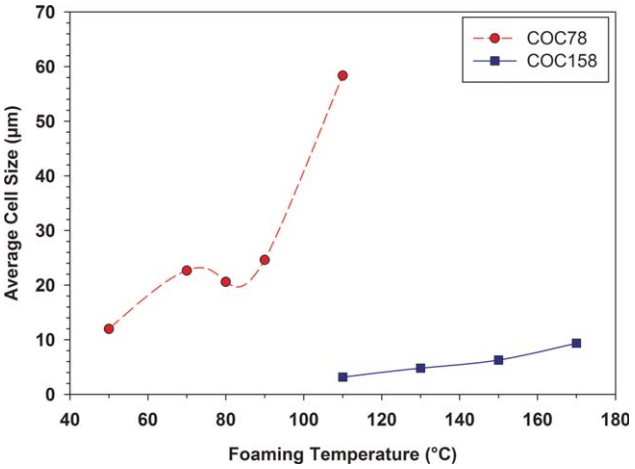

Figure 7. Average cell size at different foaming temperatures for COC78 and COC158. [Color figure can be viewed in the online issue, which is available at wileyonlinelibrary.com.]

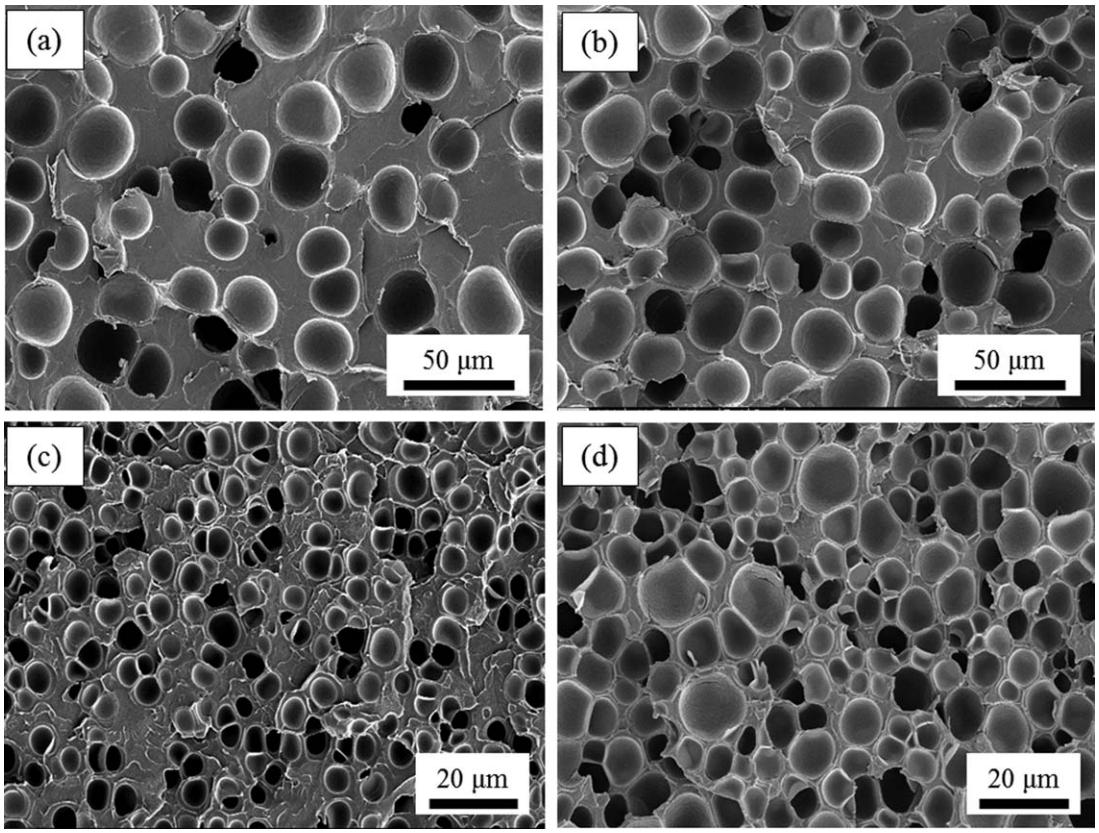

Figure 8. SEM images of COC78 foams with relative density and cell size of (a) 75%, 22.6 μm and (b) 55%, 20.6 μm; COC158 foams with relative density and cell size of (c) 78%, 4.8 μm and (d) 53%, 6.3 μm.

It can potentially be used in many applications, such as filtration membranes and battery separators.

Nanoporous structures on cell walls were previously reported in polyetherimide,[28] polycarbonate,[29] and polyethersulfone.[30] The nanoporous structures only existed on the surface of the cell wall, with solid polymer underneath the nanoporous structure and thus two neighboring microcells are not interconnected. However, in this study, the pores occupy the whole thickness of the cell wall and microcells are interconnected through these pores. The formation mechanism of the hierarchical structure is not understood at present. One possible mechanism is the stress-induced cell nucleation on the cell wall. During cell growth, the cell walls of the microcells experience a large tensile stress from the stretching. The large tensile stress can cause the residual CO_2 on the cell wall to nucleate and form new cells. The formation mechanism is currently under investigation.

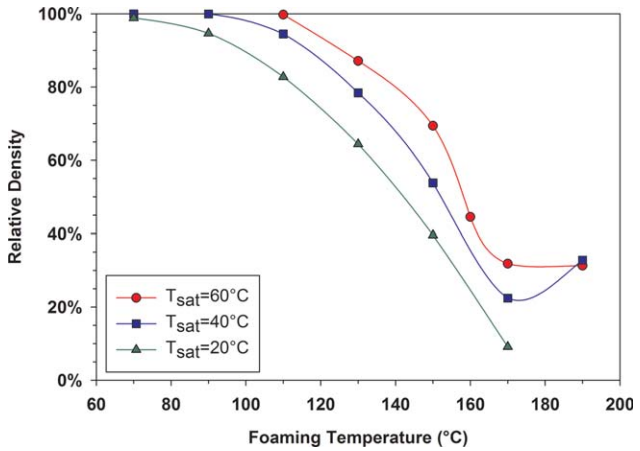

Figure 9. Relative density as a function of foaming temperatures for COC158 saturated at different saturation temperatures. [Color figure can be viewed in the online issue, which is available at wileyonlinelibrary.com.]

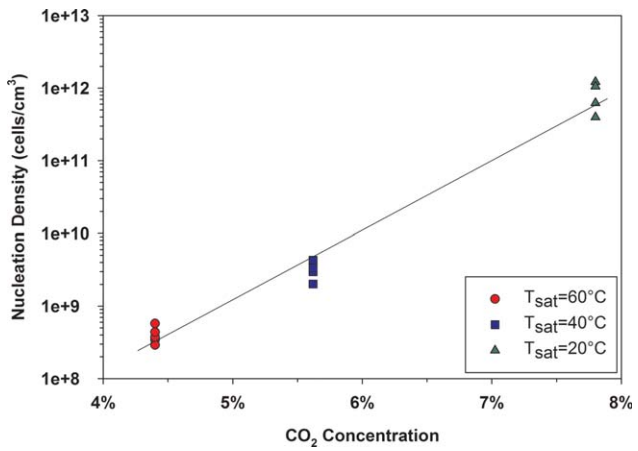

Figure 10. Nucleation density as a function of CO_2 concentration achieved via different saturation temperatures. [Color figure can be viewed in the online issue, which is available at wileyonlinelibrary.com.]

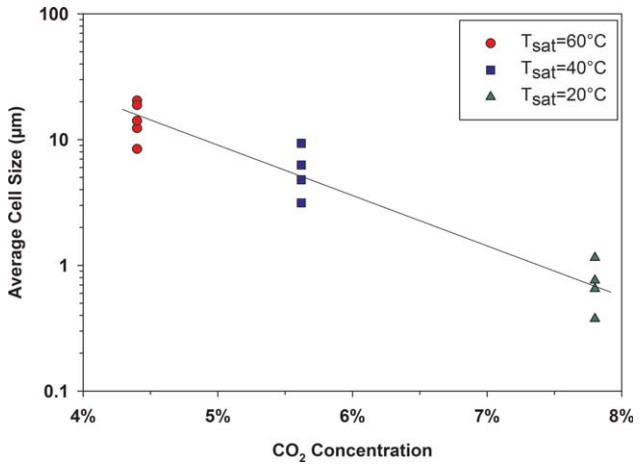

Figure 11. Average cell size as a function of CO_2 concentration achieved via different saturation temperatures. [Color figure can be viewed in the online issue, which is available at wileyonlinelibrary.com.]

SUMMARY

The effects of T_g and T_{sat} on the solid-state microcellular foaming of COC, including CO_2 solubility, diffusivity, cell nucleation, and foam morphology, were investigated in this study. COCs of low T_g (78°C) and high T_g (158°C) were used in this study. The T_gs were varied by adjusting the amount of norbornene content in the composition of copolymer, with higher norbornene content in the higher T_g COC. A temperature range of 20–80°C was chosen to study the effect of T_{sat}.

Solubilities decrease with increasing T_{sat}, and Arrhenius relationship between solubility and saturation temperature is observed for both COCs. Solubilities are 20–50% higher in high T_g COC than the low T_g COC across the saturation temperature range. Diffusivities increase with increasing T_{sat}. Diffusivities are about 15% higher on average in high T_g COC for temperatures up to 50°C. A much faster increase of diffusivity beyond 50°C is observed in low T_g COC probably due to it being in the rubbery state.

We decoupled the effect of T_g and effect of gas concentration. Relationships between relative densities and foaming temperature for COC78 and COC158 are also established. Under similar CO_2 concentration, high T_g COC starts foaming at a higher temperature. And the density decreases faster in low T_g COC with foaming temperature. Also, high T_g COC foams show about two orders of magnitude higher cell nucleation density than the low T_g COC foams, and the cells are smaller in the high T_g foams.

The effect of T_{sat} on the microcellular foaming of COC was also studied using the high T_g COC. The effect of T_{sat} can be viewed as the effect of gas concentration. As the T_{sat} decreases, the gas concentration increases. As the gas concentration increases, cell nucleation density increases and cell size decreases, both

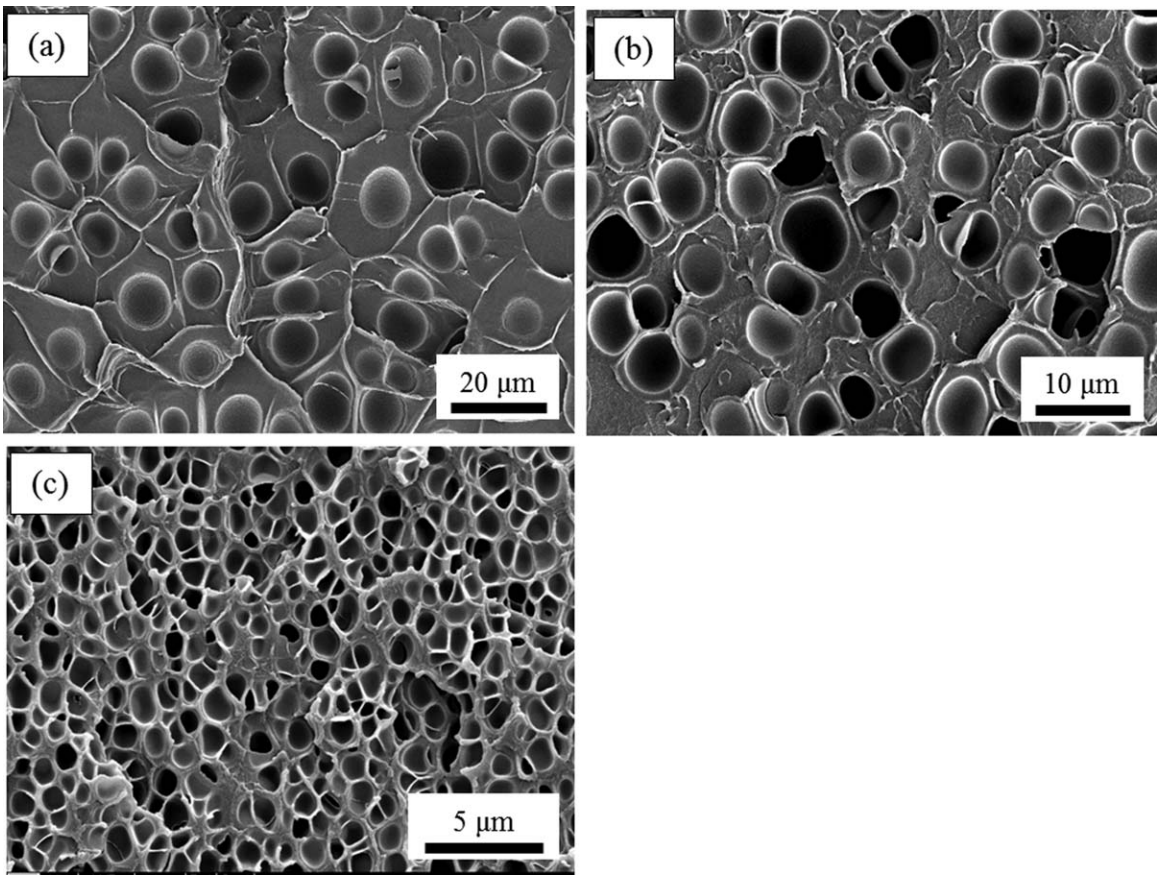

Figure 12. COC158 samples saturated at different temperatures and then foamed at 130°C: (a) $T_{sat} = 60$°C, RD 87.1%, cell size 8.4 μm; (b) $T_{sat} = 40$°C, RD 77.8%, cell size 4.8 μm; (c) $T_{sat} = 20$°C, RD 64.4%, cell size 0.76 μm.

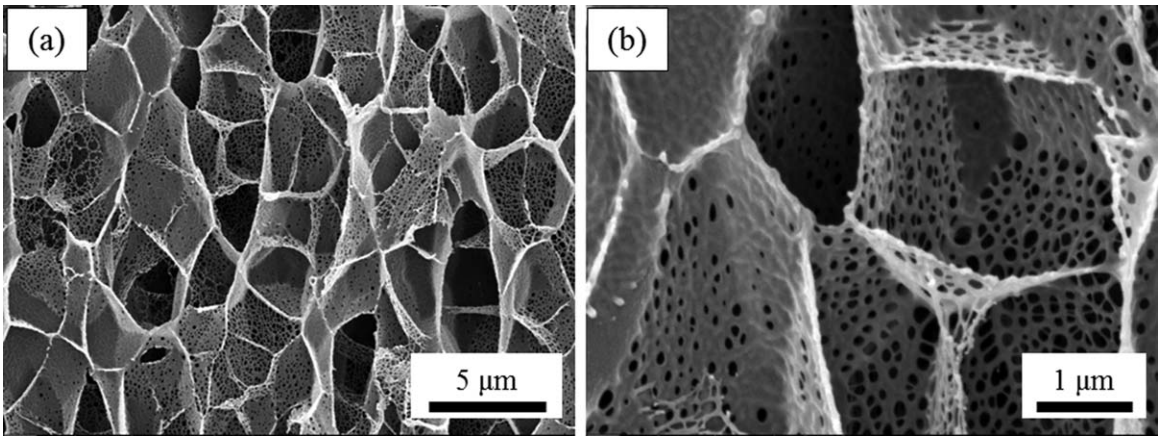

Figure 13. Hierarchical structure of low-density (9.1% relative density) COC158 foam. (b) is a close-up of (a). Cells on the cell wall are about 80 nm in diameter.

exponentially. Uniform ultramicrocellular structure with an average cell size of 380 nm was created. A novel hierarchical structure with ~2.5 μm microcells and 80 nm nanopores on the cell walls was discovered in the very low-density foams.

ACKNOWLEDGMENTS

The authors would like to thank TOPAS Advanced Polymers for providing the materials for this study, and members of the University of Washington Cellular Composites Consortium for sponsoring the project.

REFERENCES

1. Martini, J.; Suh, N.; Waldman, F. A. Microcellular closed cell foams and their method of manufacture. Patent #4473665. USA: Massachusetts Institute of Technology, **1984**.
2. Martini, J.; Waldman, F. A.; Suh, N. The production and analysis of microcellular thermoplastic foam. SPE ANTEC: San Francisco, CA: **1982**; Vol. 28. p 674.
3. Kumar, V.; Weller, J. *Int. Polym. Process.* **1993**, 73.
4. Murray, R. E.; Weller, J.; Kumar, V. *Cell. Polym.* **2000**, *19*, 413.
5. Kumar, V.; Weller, J. *J. Eng. Ind.* **1994**, *116*, 413.
6. Guo, H.; Nadella, K.; Kumar, V. *J. Mater. Res.* **2013**, *28*, 2374.
7. Richards, E.; Rizvi, R.; Chow, A.; Naguib, H. *J. Polym. Environ.* **2008**, *16*, 258.
8. Wang, X.; Kumar, V.; Li, W. *Cell. Polym.* **2007**, *26*, 1.
9. Goel, S. K.; Beckman, E. J. *Cell. Polym.* **1993**, *12*, 251.
10. Shin, J. Y.; Park, J. Y.; Liu, C.; He, J.; Kim, S. C. *Pure Appl. Chem.* **2005**, *77*, 801.
11. Krause, B.; Mettinkhof, R.; van der Vegt, N. F. A.; Wessling, M. *Macromolecules* **2001**, *34*, 874.
12. Sun, X.; Liu, H.; Li, G.; Liao, X.; He, J. *J. Appl. Polym. Sci.* **2004**, *93*, 163.
13. Gendron, R.; Champagne, M. F.; Tatibouet, J.; Bureau, M. N. *Cell. Polym.* **2009**, *28*, 1.
14. Chen, Z.; Zeng, C.; Yao, Z.; Cao, K. *Ind. Eng. Chem. Res.* **2013**, *52*, 9381.
15. Crank, J.; Park, G. S. *Diffusion in Polymers*; Academic Press: London, **1968**.
16. Handa, Y. P.; Zhang, Z.; Wong, B. *Cell. Polym.* **2001**, *20*, 1.
17. Guo, H.; Kumar, V. Solid-State Microcellular Foaming of Low- and High-T_g Cyclic Olefin Copolymer (COC), SPE FOAMS 2014 Conference, Iselin, NJ, **2014**.
18. Kumar, V.; Weller, J. E. *J. Eng. Ind.* **1994**, *116*, 413.
19. Kumar, V.; Suh, N. *Polym. Eng. Sci.* **1990**, *30*, 1323.
20. Hu, C.; Lee, K.; Ruaan, R.; Jean, Y.; Lai, J. *J. Membr. Sci.* **2006**, *274*, 192.
21. Guo, H.; Kumar, V. *Polymer* **2015**, *56*, 46.
22. Pantoula, M.; Panayiotou, C. *J. Supercrit. Fluids* **2006**, *37*, 254.
23. Guo, H.; Kumar, V. *Polymer* **2015**, *57*, 157.
24. Crank, J. *The Mathematics of Diffusion*; Oxford Science Press: New York, **1989**.
25. Barrer, R. M. *Nature* **1937**, *140*, 106.
26. Meares, P. *J. Am. Chem. Soc.* **1954**, *76*, 3415.
27. Handa, Y. P.; Wong, B.; Zhang, Z. *Polym. Eng. Sci.* **1999**, *39*, 55.
28. Miller, D.; Kumar, V. *Polymer* **2009**, *50*, 5576.
29. Fukasawa, Y.; Chen, J.; Saito, H. *J. Polym. Sci. Part B Polym. Phys.* **2008**, *46*, 843.
30. Sorrentino, L.; Aurilia, M.; Iannace, S. *Adv. Polym. Technol.* **2011**, *30*, 234.